CellPress

Cancer Cell
Article

Postsurgical Adjuvant Tumor Therapy by Combining Anti-Angiopoietin-2 and Metronomic Chemotherapy Limits Metastatic Growth

Kshitij Srivastava,[1,7] Junhao Hu,[1,7] Claudia Korn,[1] Soniya Savant,[1,2] Martin Teichert,[1,2] Stephanie S. Kapel,[1] Manfred Jugold,[3] Eva Besemfelder,[1] Markus Thomas,[4] Manolis Pasparakis,[5] and Hellmut G. Augustin[1,2,6,*]

[1]Division of Vascular Oncology and Metastasis, German Cancer Research Center Heidelberg (DKFZ-ZMBH Alliance), 69121 Heidelberg, Germany

[2]Department of Vascular Biology and Tumor Angiogenesis (CBTM), Medical Faculty Mannheim, Heidelberg University, 68167 Mannheim, Germany

[3]Small Animal Imaging Center, German Cancer Research Center Heidelberg, Heidelberg, Germany

[4]Roche Diagnostics, GmbH, 82377 Penzberg, Germany

[5]Institute for Genetics, Center for Molecular Medicine (CMMC), and Cologne Excellence Cluster on Cellular Stress Responses in Aging-Associated Diseases (CECAD), University of Cologne, 50923 Cologne, Germany

[6]German Cancer Consortium, 69120 Heidelberg, Germany

[7]Co-first author

*Correspondence: augustin@angiogenese.de

http://dx.doi.org/10.1016/j.ccell.2014.11.005

SUMMARY

Antiangiogenic tumor therapy has failed in the adjuvant setting. Here we show that inhibition of the Tie2 ligand angiopoietin-2 (Ang2) effectively blocks metastatic growth in preclinical mouse models of postsurgical adjuvant therapy. Ang2 antibody treatment combines well with low-dose metronomic chemotherapy (LDMC) in settings in which maximum-dose chemotherapy does not prove effective. Mechanistically, Ang2 blockade could be linked to quenching the inflammatory and angiogenic response of endothelial cells (ECs) in the metastatic niche. Reduced EC adhesion molecule and chemokine expression inhibits the recruitment of tumor-promoting $CCR2^{+}Tie2^{-}$ metastasis-associated macrophages. Moreover, LDMC contributes to therapeutic efficacy by inhibiting the recruitment of protumorigenic bone marrow-derived myeloid cells. Collectively, these data provide a rationale for mechanism-guided adjuvant tumor therapies.

INTRODUCTION

Surgery is the standard care of treatment for resectable primary tumors. However, many cancer patients experience fatal metastatic growth despite removal of the primary tumor. For instance, 30% of node-negative and 70% of node-positive breast cancer patients succumb to distant metastases despite surgical intervention (Demicheli et al., 2008), confirming the well-established fact that metastatic seeding has already occurred at the time of diagnosis and subsequent surgery. Hence, better and preferably mechanism-based clinical regimens of postsurgical adjuvant therapy need to be developed to follow surgery, even when no metastases are evident, to lower the risk that the cancer will come back.

Antiangiogenic tumor therapies, targeting the VEGF pathway, have received widespread clinical application for the treatment of advanced primary tumors. Their efficacy is still limited, and antiangiogenic primary tumor therapy has in preclinical models even been proposed to promote metastasis (Ebos et al., 2009; Pàez-Ribes et al., 2009). In the adjuvant setting, anti-VEGF therapy did not prove clinically effective, as shown in colorectal cancer (Allegra et al., 2011; de Gramont et al.,

Significance

There is an unmet need for safe and effective forms of adjuvant tumor therapy following surgical removal of primary tumors, particularly in patients with nonovert, undetectable metastases that would be excluded from more aggressive forms of adjuvant therapy (radiotherapy, chemotherapy). This study has identified the combination of an anti-Ang2 antibody and LDMC as a promising low-adverse effect combination therapy for such setting. Moreover, the study provides mechanistic insights into the endothelial contribution of a proinflammatory microenvironment as an important mediator of tumor progression, which is targeted by the combination therapy of anti-Ang2 antibody and LDMC. These data warrant further preclinical validation of such combination therapy for eventual translation into clinical application.

2012) as well as in triple-negative breast cancer (Cameron et al., 2013).

The Tie2 ligand angiopoietin-2 (Ang2) has recently emerged as a promising target for second-generation antiangiogenic drug development that can be combined with established anti-VEGF/VEGFR therapies (Gerald et al., 2013; Hashizume et al., 2010; Koh et al., 2010). Ang2 is produced by activated endothelial cells (ECs) to facilitate vascular responses to angiogenic and other endotheliotropic cytokines. In fact, Ang2 upregulation may be among the first cellular responses of angiogenic activation to contribute toward the vascular priming associated with the induction of angiogenesis (Holash et al., 1999; Zagzag et al., 1999).

On the basis of its endothelial activation-associated transcriptional regulation, we hypothesized that Ang2 may be an attractive target for postsurgical adjuvant therapy. Conceptually, Ang2-targeting therapies should quench the vascular response and thereby prevent the growth of seeded metastases. To probe this hypothesis, we used two different models of spontaneous metastasis (including an anti-VEGF-refractory model) in which adjuvant therapy was initiated following surgical removal of the primary tumor. Comparatively, we also studied the efficacy of anti-VEGF antibody (VEGF Ab), maximum-tolerated-dose chemotherapy (MTDC), and low-dose metronomic chemotherapy (LDMC) in the same models. The results of these preclinical therapy experiments guided experiments aimed at unraveling the underlying mechanisms to pave the way for mechanism-guided postsurgical adjuvant combination tumor therapies.

RESULTS

Anti-Ang2 Therapy Limits the Growth of Preseeded Micrometastases

To study the effect of Ang2-targeting in the adjuvant setting, we used an orthotopic breast cancer model, which closely mimics lung and bone metastasis as frequently observed during human breast cancer progression (Figure 1A). Ang2 Ab therapy reduced the incidence of bone metastases as well as the growth of lung metastases in the 4T1 breast cancer mouse model (Figures 1B–1G). Exclusion of residual primary tumor growth after surgery (before randomization to treatment groups) (Figure S1A available online) and the decrease in metastatic burden upon therapy was traced by bioluminescence imaging (Figure 1B). Bone metastases were more frequent in the control group (seven of ten versus two of ten) (Figure 1C). Representative images of hematoxylin and eosin (H&E) sections with osteolytic lesions displayed the extent of bone damage inflicted by metastasis (Figure 1D). The lesions caused a corresponding loss of bone density, which was further confirmed by computed tomographic (CT) imaging (Figure 1E). Bioluminescence imaging also revealed reduced lung and lymph node metastasis upon Ang2 blockade (Figures 1B and 1C). H&E sections of lungs identified a significantly decreased incidence of macrometastases (Figures 1F and 1G) and micrometastases (Figures S1B and S1C) in Ang2 Ab-treated mice. Ang2 blockade resulted in a significant decrease of vessel density and increase of intratumor microvessel pericyte coverage compared to the immunoglobulin G (IgG)-treated control group (Figures 1H–1J).

Metronomic Chemotherapy Increases the Antimetastatic Effect of Anti-Ang2 Ab and Promotes Overall Survival

Although Ang2 blockade reduced metastatic growth, residual metastasis was detected upon bioluminescent imaging. This led us to hypothesize that an additional therapeutic regimen may improve the therapeutic benefit conferred by Ang2 blockade. To test this hypothesis, we combined low-dose paclitaxel metronomic chemotherapy [LDMC(PTX)] with Ang2 Ab therapy in the postsurgical adjuvant setting of the 4T1 orthotopic breast cancer model. The combinatorial therapy was significantly more effective than either LDMC (PTX) or MTDC (PTX) given as monotherapy (Figures 2A and 2B). Interestingly, Ang2 targeting alone yielded a significantly better therapeutic response than MTDC (PTX).

Next, we investigated whether the therapeutic benefit conferred by combinations of Ang2 Ab and LDMC (PTX) would also translate to improved overall survival. Combinations of Ang2 Ab and LDMC (PTX) significantly increased overall survival compared with Ang2 Ab alone or control IgG (mean survival of LDMC (PTX) plus Ang2 Ab versus Ang2 Ab alone: 33.5 versus 27 days, $p < 0.04$; mean survival of LDMC (PTX) plus Ang2 Ab versus IgG: 33.5 versus 25 days, $p < 0.0001$; Figure 2C). In contrast to this combination, MTDC (PTX) alone failed to provide any survival benefit (Figure 2C).

LDMC and Anti-Ang2 Ab Combination Therapy Has Fewer Adverse Effects Than High-Dose Chemotherapy

MTDC (PTX) is clinically frequently used as postsurgical adjuvant chemotherapy. We thus analyzed the adverse effects of the different therapeutic regimens used in this study. Histological analysis revealed severe bone marrow suppression in the MTDC (PTX) group (Figure 2D). Reproductive toxicity is a major adverse effect often observed in female breast cancer patients undergoing chemotherapy subsequent to mastectomy. MTDC (PTX) resulted in significantly fewer healthy follicles compared with control or other therapeutic regimens (Figure 2E). Lastly, a significant reduction in body weight was observed in the MTDC (PTX) group, but not in the other treatment groups, including the combination of LDMC (PTX) and Ang2 Ab (Figure 2F).

Anti-Ang2 Ab Therapy Inhibits Metastatic Growth in an Anti-VEGF-Refractory Tumor Model

Following the demonstration of the effect of Ang2 Ab on metastatic growth in the 4T1 orthotopic breast cancer model, we next conducted experiments aimed at examining the effect of Ang2 blockade on the growth of micrometastases in the Lewis lung carcinoma (LLC) model (Figure 3A). Subcutaneously growing LLCs, previously shown to be refractory to anti-VEGF therapy (Shojaei et al., 2007a), were removed at approximately 0.30 g (day 14 following inoculation). No visible metastases were macroscopically detectable at this stage. Intriguingly, primary tumor removal led to the rapid downregulation of circulating VEGF levels (Figure S2).

Postsurgical adjuvant Ang2 Ab therapy inhibited the growth of LLC metastases in the lungs. Macroscopic metastases were detected in 80% of control IgG-treated mice, whereas only 20% of Ang2 Ab-treated mice had macroscopic metastases

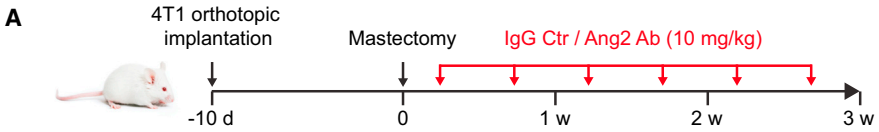

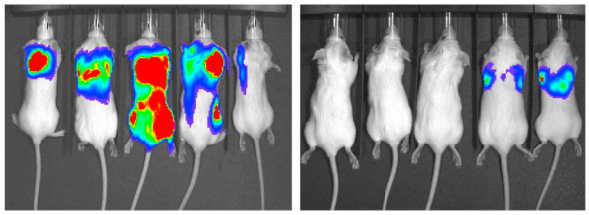

C

	Total number of mice	Metastasis		
		Lung	Bone	Lymph node
IgG	10	10	7	6
Ang2 Ab	10	4	2	3

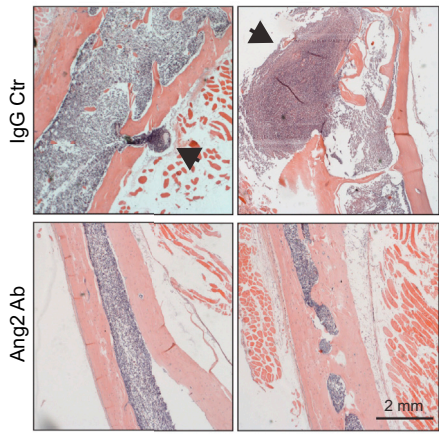

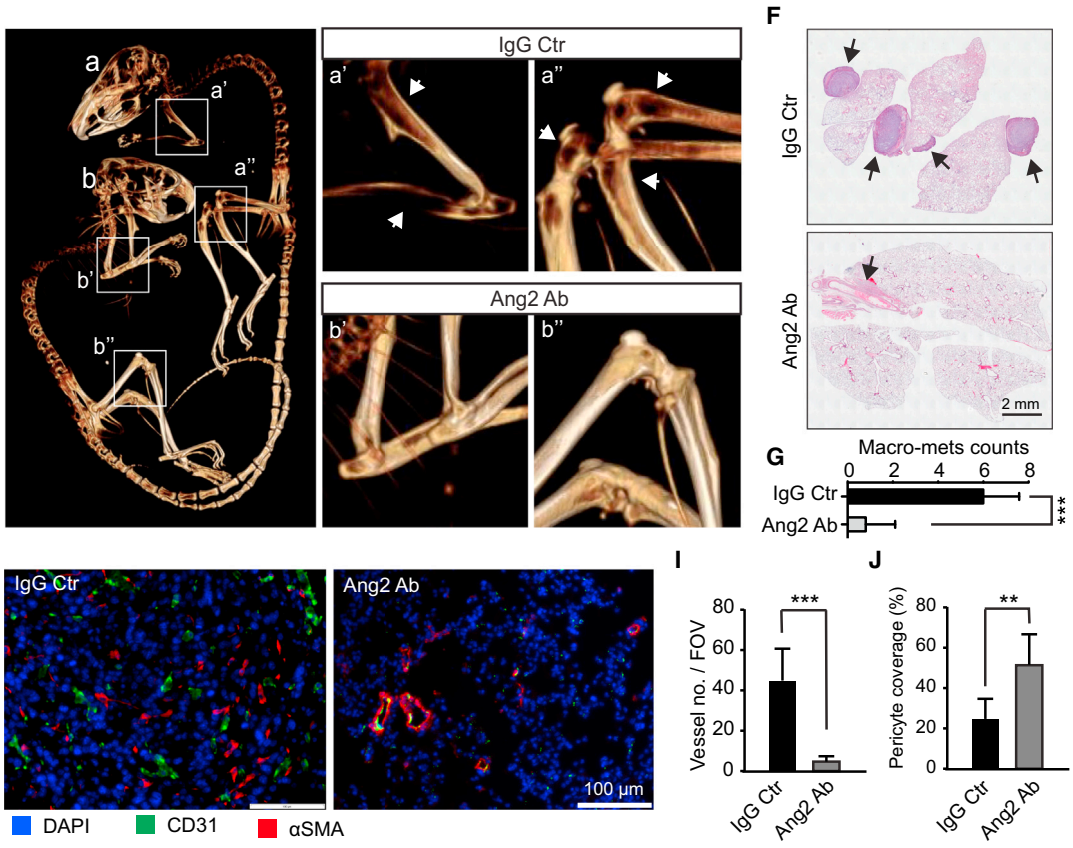

Figure 1. Adjuvant Ang2 Blockade Inhibits Metastatic Growth of Orthotopic 4T1 Mammary Tumors

(A) Schematic representation of the experimental protocol. 4T1 tumors grown orthotopically in the third right mammary fat pad were surgically removed after 10 days (average tumor size 250 mm^3), following which therapy was initiated with the Ang2 Ab or control IgG. Mice were sacrificed after 3 weeks of treatment.

(B) Bioluminescence imaging 3 weeks after primary tumor removal.

(C) Table enumerating frequency of metastatic lesions in various organs (from two experiments).

(D) Representative images showing H&E-stained bone sections. Black arrows indicate osteolytic lesions and associated periosteal discontinuity.

(legend continued on next page)

(Figure 3B). H&E staining of lung sections confirmed the significant reduction of metastatic growth in the Ang2 Ab-treated group compared with control IgG-treated mice (Figures 3C and 3D).

Metronomic Chemotherapy Increases the Antimetastatic Efficacy of Ang2 Targeting in an Anti-VEGF-Refractory Model

As Ang2 inhibition blocked growth of micrometastases in the anti-VEGF-refractory LLC model, we next compared the efficacy of the Ang2 Ab with a neutralizing VEGF Ab in the postsurgical adjuvant setting. Moreover, as resistance to VEGF/VEGFR2 targeting has been attributed to the recruitment of $Cd11b^{+}Gr1^{+}$ or $Cd11b^{+}Gr1^{+}Ly6C^{hi}$ cells in this tumor model (Priceman et al., 2010; Shojaei et al., 2007a), we evaluated the efficacy of paclitaxel in inhibiting the recruitment of these cells to sites of metastasis. To that end, we compared paclitaxel with another standard chemotherapy, gemcitabine, because the latter has been shown to interfere with recruitment of these cells at MTD in primary tumor models (Suzuki et al., 2005). Gemcitabine even at metronomic dosing inhibited recruitment of the resistance-conferring myeloid cells more effectively than paclitaxel (Figures S3A and S3B) in the LLC model. Thus, along with Ang2 Ab and VEGF Ab, we evaluated their combination with metronomic gemcitabine [LDMC(GEM)] and MTD gemcitabine [MTDC(GEM)] for inhibition of postsurgical metastases.

Postsurgical adjuvant Ang2 Ab therapy inhibited the growth of LLC metastases in the lungs, in contrast to VEGF Ab therapy, which showed extensive metastatic growth (Figures 4A and 4B). LDMC (GEM) inhibited metastatic growth more effectively than MTDC (GEM). H&E staining of tissues sections confirmed the significant reduction of metastatic growth by the combination of Ang2 Ab with VEGF Ab and metronomic chemotherapy compared with the other treatment groups (Figures 4A and 4B).

Ang2 Neutralization Inhibits Angiogenesis in Growing Metastatic Nodules

Resistance to anti-VEGF agents has been associated with the formation of a nonresponsive refractory vasculature in response to cytokines from resistance-conferring myeloid cells (Helfrich et al., 2010; Shojaei et al., 2009). Analysis of the vasculature in metastatic nodules revealed a significantly reduced vessel area upon Ang2 Ab treatment compared with IgG- or VEGF Ab-treated animals (Figures 4C and 4D). IgG-treated mice had primarily medium-size vessels (100–1,600 μm^2) with a pericyte coverage of 22% (Figures 4E and 4F). The remaining vessels in metastases of Ang2 Ab-treated mice were smaller (<100 μm^2) but more stable, as indicated by increased coverage with pericytes (Figures 4C–4F). The reduced vascularization of Ang2 Ab-treated mice correlated with increased tissue hypoxia as indicated by increased Hif1α staining compared with IgG-treated mice (Figures S3C and S3D). In contrast to Ang2 Ab treatment, mice treated with VEGF Ab had predominantly large vessels (>400 μm^2) with poor pericyte coverage (Figures 4E and 4F). Hif1α immunoreactivity was more intense in VEGF Ab-treated lung metastases compared with IgG control (Figures S3C and S3D).

Ang2 Controlled Endothelial CCL2 Induction Leads to the Recruitment of $CCR2^{+}$ Metastasis-Associated Macrophages

In order to unravel the underlying mechanisms of the antimetastatic effect of Ang2 Ab treatment in the postsurgical adjuvant setting, we examined the stromal inflammatory infiltration of metastases. Immunohistochemical staining of lung metastases revealed more F4/80-positive macrophages in the IgG control group than in the Ang2 Ab-treated animals (Figure 5A). Flow cytometric analyses of lung metastases-derived cell suspensions identified the inflammatory infiltrate as CCR2-positive and Tie2-negative metastasis-associated macrophages (MAMs) ($CCR2^{+}Tie2^{-}$ MAMs) (Qian and Pollard, 2010). Both the total number of macrophages and the fraction of $CCR2^{+}Tie2^{-}$ MAMs were significantly decreased in the Ang2 Ab-treated group (Figures 5B, 5C, and S4A). The fraction of Tie2-positive macrophages did not differ significantly in IgG- or Ang2 Ab-treated animals (Figure S4B).

In order to validate the Ang2 dependency of the CCR2-positive macrophage recruitment, we performed a Matrigel plug assay using postsurgical serum from IgG- or Ang2 Ab-treated mice as stimulus. Corroborating the results of the flow cytometric analyses, immunofluorescence staining was consistent with Ang2 dependency of the influx of CCR2-positive macrophages. Furthermore, when the plug was spiked with the CCR2 ligand CCL2 in addition to serum from Ang2 Ab-treated mice, significantly more macrophages were recruited than with the serum alone (Figure 5D). Next, we investigated the mechanism underlying Ang2-dependent recruitment of MAMs to metastases. CCL2 is required for the recruitment of CCR2-positive MAMs. Ang2 stimulation of cultured human umbilical vein ECs (HUVECs) led to upregulation of endothelial *CCL2* expression, consistent with the Ang2 dependency of CCR2+ macrophage recruitment in vivo (Figure 5E). These findings were confirmed in the 4T1 tumor model revealing that Ang2 Ab treatment resulted in significantly reduced CCL2 levels in both the serum as well as lung metastases compared with IgG control treatment (Figures 5F,

(E) Representative CT images of mouse skeletons (left: overview of simultaneously scanned samples from both treatment groups; right: comparative images of high magnifications of long bone samples from control IgG-treated mice [a′,a″] and Ang2 Ab-treated mice [b′,b″]). White arrows mark osteolytic lesions.
(F) Representative low-magnification H&E-stained lung sections from both treatment groups. Black arrows mark macrometastases.
(G) Quantification of frequency of metastases in lungs expressed as number of macrometastatic lesions (>1 mm in diameter) per total lung section (n = 5 mice; three independent experiments; $^{***}p \leq 0.001$).
(H) Representative immunohistochemical images of CD31- and αSMA-stained lung metastases to visualize blood vessels (CD31) and mural cells (αSMA).
(I and J) Quantification of (I) microvessel density (expressed as vessel number per microscopic field of view [FOV]) and (J) vessel maturation (expressed as percentage of αSMA-positive CD31 microvessels compared with the total number of CD31 microvessels) in lung metastases of control IgG- and Ang2 Ab-treated mice.
Values are mean ± SD; n = 5 mice; $^{**}p \leq 0.01$, $^{***}p \leq 0.001$. The experiment was repeated three times. The figure shows representative images from one of the experiments. See also Figure S1.

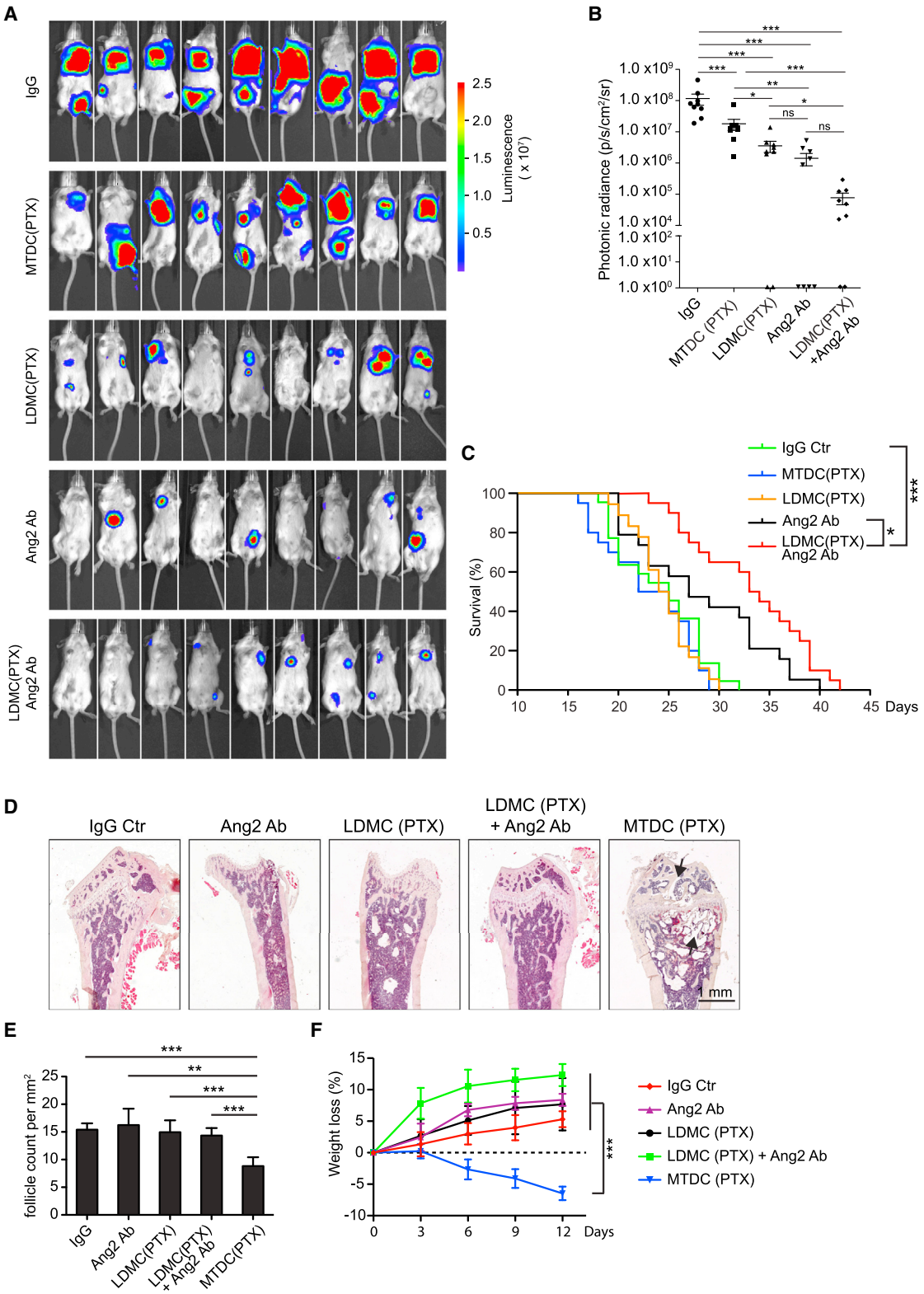

Figure 2. Comparative Analysis of Adjuvant Therapeutic Regimens in the Orthotopic 4T1 Breast Cancer Model

Therapeutic regimens: IgG Ctrl = control IgG; MTDC (PTX) = MTD paclitaxel chemotherapy; LDMC (PTX) = low-dose metronomic paclitaxel chemotherapy; Ang2 Ab = anti-Ang2 Ab treatment; LDMC (PTX) + Ang2 Ab = combination of the two treatments.

(A) Images from bioluminescence analysis 3 weeks after mastectomy to evaluate the efficacy of different therapeutic modalities.

(legend continued on next page)

S4C, and S4D). The cytokine array also identified TREM-1 as another prominently regulated molecule upon Ang2 blockade. However, further analysis established it as nonendothelial and of myeloid origin (Figures S4D and S4E).

Genetic Depletion of CCR2 or Neutralization of CCL2 Postsurgically Reduces Metastatic Growth

In order to validate the importance of Ang2-induced CCL2/CCR2-dependent macrophage recruitment during metastatic growth, two independent experimental approaches targeting either the ligand CCL2 or the macrophage receptor CCR2 were applied. Upon CCL2 neutralization with a neutralizing Ab in an adjuvant setting of 4T1 orthotopic breast cancer, lung metastases were significantly decreased compared with IgG-treated animals, as quantified by ex vivo bioluminescence measurements (Figures 5G–5I). Furthermore, the CCR2 receptor was conditionally deleted in myeloid cells in vivo, after surgical removal of the primary tumor in the syngeneic LLC model by treating *Ccr2*$^{fl/fl}$::*Mx1 Cre* with Poly I:C (Figures 5J and S4F). The postsurgical deletion of CCR2 led to a significant decrease in lung macrometastases compared with control mice (Figure 5K and 5L). These results support a role of Ang2-CCL2-CCR2 axis for metastatic growth.

To investigate the clinical relevance of the observed Ang2-controlled CCL2-dependent metastatic growth in mice, we evaluated the correlation of *CCL2* and *Ang2* expression level in a breast cancer patient data set. The mRNA data scattered strongly in the random clinical cohorts. Yet whereas *Ang2* expression levels did not correlate with *CCL2* expression in the grade 1 patient samples ($r = 0.082$, $p = 0.51$), there was a significant correlation between *Ang2* and *CCL2* expression in grade 2 and 3 patient samples ($r = 0.388$, $p = 0.0012$).

Ang2 Controls Inflammatory Adhesion Molecule Expression

Having demonstrated Ang2-dependent CCL2 upregulation and recruitment of CCR2-positive MAMs, we next investigated whether Ang2 also contributes to the formation of a prometastatic microenvironment by positively regulating inflammatory adhesion molecule expression favoring homing of MAMs to the metastases. Quantitative RT-PCR analyses of lung lysates 24 hr after tail vein injection of LLC cells identified a decrease of *Icam-1* expression in Ang2 Ab-treated mice to 40% of IgG-treated animals (Figure 6A). The downregulation of *Icam-1* mRNA expression by Ang2 Ab was confirmed by western blot analysis of lung metastases lysates from mice treated with Ang2 Ab or control IgG (Figures 6B and 6C). Similarly, *Vcam-1* expression was decreased in the postsurgical adjuvant LLC model upon Ang2 Ab treatment (Figure S5A).

In order to analyze the functional relevance of decreased adhesion molecule expression upon Ang2 Ab therapy, we performed flow chamber assays with cultured ECs (HUVECs). Pretreatment of HUVECs with Ang2 Ab resulted in significantly reduced adhesion and increased rolling velocity of macrophages over cultured HUVECs (Figures 6D and 6E; Movies S1 and S2). In order to confirm that the changes in rolling velocity could be attributed to different expression levels of Ang2-regulated ICAM-1, we performed flow chamber experiments with ICAM-1 Ab- or IgG-coated microspheres using HUVEC-seeded chambers with or without Ang2 Ab pretreatment. The rolling velocity of ICAM-1 Ab-coated microspheres in the HUVEC-seeded chambers was significantly increased upon pretreatment with Ang2 Ab, consistent with an Ang2-dependent mechanism of ICAM-1 upregulation (Figures 6F and 6G; Movies S3 and S4). The identified Ang2-controlled ICAM-1 expression could be potentially clinically relevant, because Ang2 and ICAM-1 expression levels significantly correlated in grades 2 and 3 but not in grade 1 breast cancer patient samples (Figure S5B).

Endothelial Activation by Ang2 Leads to ICAM-1 Upregulation in a STAT3- and NF-κB-Dependent Manner

Adhesion molecules are classically known to be downstream targets of inflammatory signaling pathways. Angiogenic stimuli induce activation of STAT3 pathway by regulating nuclear translocation of phospho-Tyr705-STAT3 (Yahata et al., 2003). We hypothesized that Ang2 may similarly induce such pathways in ECs and thereby regulate expression of ICAM-1. Phosphorylation of STAT3 leads to its nuclear translocation. Hence, we investigated the localization of phospho-STAT3 in HUVECs by immunofluorescence staining. Phospho-STAT3 was detected at low levels in the cytoplasm but not in the nuclei of unstimulated HUVECs. However, upon Ang2 stimulation, STAT3 was phosphorylated and translocated to the nucleus (Figures 6H–6J). To assess the functional relevance of STAT3 activation in the Ang2-mediated upregulation of ICAM-1, we next exploited a cell-permeable STAT3-specific inhibitory peptide (Turkson et al., 2001). Ang2-mediated upregulation of ICAM-1 was inhibited in the presence of the STAT3 inhibitory peptide, while the control peptide had no effect (Figures S5C and S5D).

We also explored the significance of the NF-κB pathway in Ang2-mediated endothelial activation, because both STAT signaling and NF-κB pathways have been shown to act synergistically. Ang2 itself did not induce p65 nuclear translocation but increased TNF-α-mediated endothelial NF-κB activation, as evidenced by IκBα phosphorylation and nuclear translocation (Figures S5G and S5H). Correspondingly, Ang2 upregulated ICAM-1 in TNF-α-primed ECs (Figures S5E and S5F). Taken

(B) Quantitative bioluminescent analysis of metastatic burden in the different treatment groups (values are mean ± SEM; n = 9 mice; p/s/cm^2/sr = photons/s/cm^2/steradian).
(C) Kaplan-Meier survival curves of primary tumor resected 4T1 tumor-bearing mice treated after surgery with respective therapeutic regimens (n = 19–22 mice; log-rank test).
(D) Representative images of H&E-stained sections of bone marrow as readout of myelosuppression. The black arrow indicates hypocellular area.
(E) Evaluation of ovarian toxicity as indicated by mean numbers of healthy follicles per square millimeter (n = 4 mice).
(F) Analysis of body weight loss over time as a measure of systemic well-being of the mice.
Values are mean ± SD unless otherwise indicated; n = 4 mice; *$p \leq 0.05$, **$p \leq 0.01$, ***$p \leq 0.001$, ns = nonsignificant. Each experiment was performed twice except the survival analysis, which was done once; data from one representative experiment are presented in the figure.

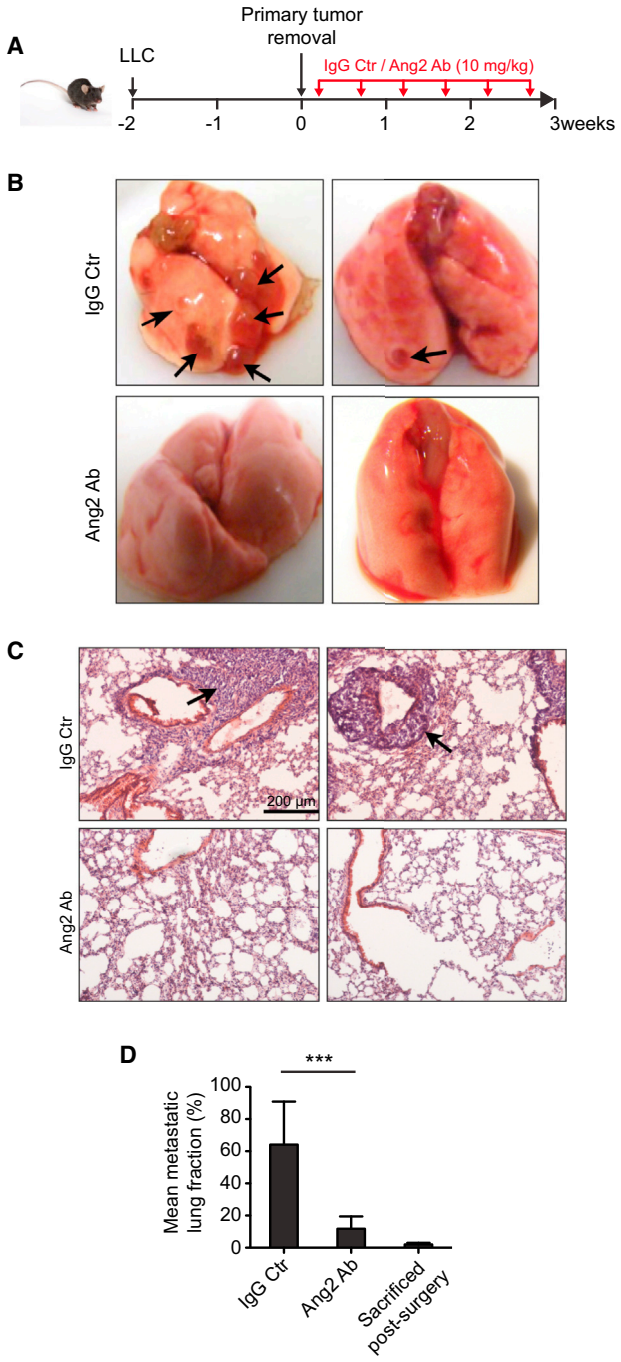

Figure 3. Effect of Ang2 Ab on Postsurgical Growth of Preseeded LLC Metastases

(A) Schematic representation of experimental protocol. Primary tumors (subcutaneous LLC tumors) were grown for 14 days, after which they were surgically removed (average tumor size 360 mm^3), and therapy was initiated thereafter. Mice were sacrificed 3 weeks after surgery.

(B) Representative images of lungs isolated from mice after sacrifice. Approximately 80% of control IgG-treated mice had macroscopically detectable lung metastases (arrows). In contrast, fewer than 20% of Ang2 Ab-treated mice had detectable metastatic foci.

(C) Representative histological images of lung sections (H&E staining) showing prominent metastatic foci in IgG-treated controls and no detectable metastases in Ang2 Ab-treated mice.

(D) Quantification of mean metastatic lung fraction analyzed by digitized image analysis using Fiji software. Mice carried small but histologically detectable micrometastases at the time of surgery, which marked the beginning of therapy (third bar).

Values are mean ± SD; n = 5 mice; ***p ≤ 0.001. The figure shows representative images from one of three independent experiments. See also Figure S2.

together, these findings are consistent with ICAM-1 upregulation by Ang2 in ECs being mediated by the synergistic activities of NF-κB and STAT3 signaling.

Metronomic Chemotherapy, but Not Anti-Ang2 Ab Therapy, Decreases the Mobilization of Resistance-Conferring Myeloid-Derived $Cd11b^+Gr1^+Ly6C^{hi}$ Cells

Metronomic chemotherapy could extend the therapeutic benefit of Ang2 blockade in both tumor models. In order to study the mechanism of the improved efficacy of the LDMC (PTX) plus Ang2 Ab combination therapy, we evaluated the effect of LDMC (PTX) on the recruitment of CD133+VEGFR2+ myeloid cells in the 4T1 orthotopic breast cancer model. LDMC monotherapy and combination therapy resulted in a significant reduction of recruited myeloid cells compared with all other treatments. Ang2 Ab had no effect on mobilization compared with the IgG-treated group, consistent with an effect of LDMC treatment (Figure S6A).

A subset of myeloid cells characterized by expression of $Cd11b^+Gr1^+$ or $Cd11b^+Gr1^+Ly6C^{hi}$ has recently been associated with conferring resistance against anti-VEGF and anti-VEGFR2 agents in preclinical studies (Priceman et al., 2010; Shojaei et al., 2007a). LDMC (GEM) was found to be more effective than paclitaxel in inhibiting the recruitment of these cells to metastases. We therefore examined if the therapeutic benefit upon gemcitabine addition to antiangiogenic therapy in the VEGF Ab refractory LLC model could, at least in part, be attributed to this observation. To this end, we evaluated the effect of various combinations and monotherapies on the recruitment of these cells to metastases. Antiangiogenic monotherapy by neutralizing VEGF or Ang2 or their combination did not inhibit the recruitment of $Cd11b^+Gr1^+$ or $Cd11b^+Gr1^+Ly6C^{hi}$ cells, whereas LDMC (GEM) or its combination with antiangiogenic regimens significantly reduced the recruitment of the resistance mediating myeloid cells to the metastases. Metronomic dosage was similarly efficacious as MTD (GEM) in inhibiting recruitment of these cells, as revealed by flow cytometric analysis of cell suspensions from lung metastases (Figures 7A, 7B, and S6B).

Myeloid cell mobilization occurs as a direct result of systemic GCSF levels. We therefore evaluated circulating concentrations GCSF. LDMC (GEM) as well as MTDC (GEM) decreased the circulating levels of GCSF, consistent with their efficacy in inhibiting mobilization of $Cd11b^+Gr1^+Ly6C^{hi}$ cells compared with antiangiogenic therapies (Figure 7C).

Anti-Ang2 Ab Inhibits Bv8/PK-2-Induced Angiogenesis

Ang2 neutralization significantly decreased angiogenesis in metastases but did not affect the recruitment of resistance-conferring proangiogenic $Cd11b^+Gr1^+$ cells in the VEGF Ab-refractory LLC model. Bv8/Pk-2 has been characterized as myeloid-derived proangiogenic cytokine mediating angiogenesis in

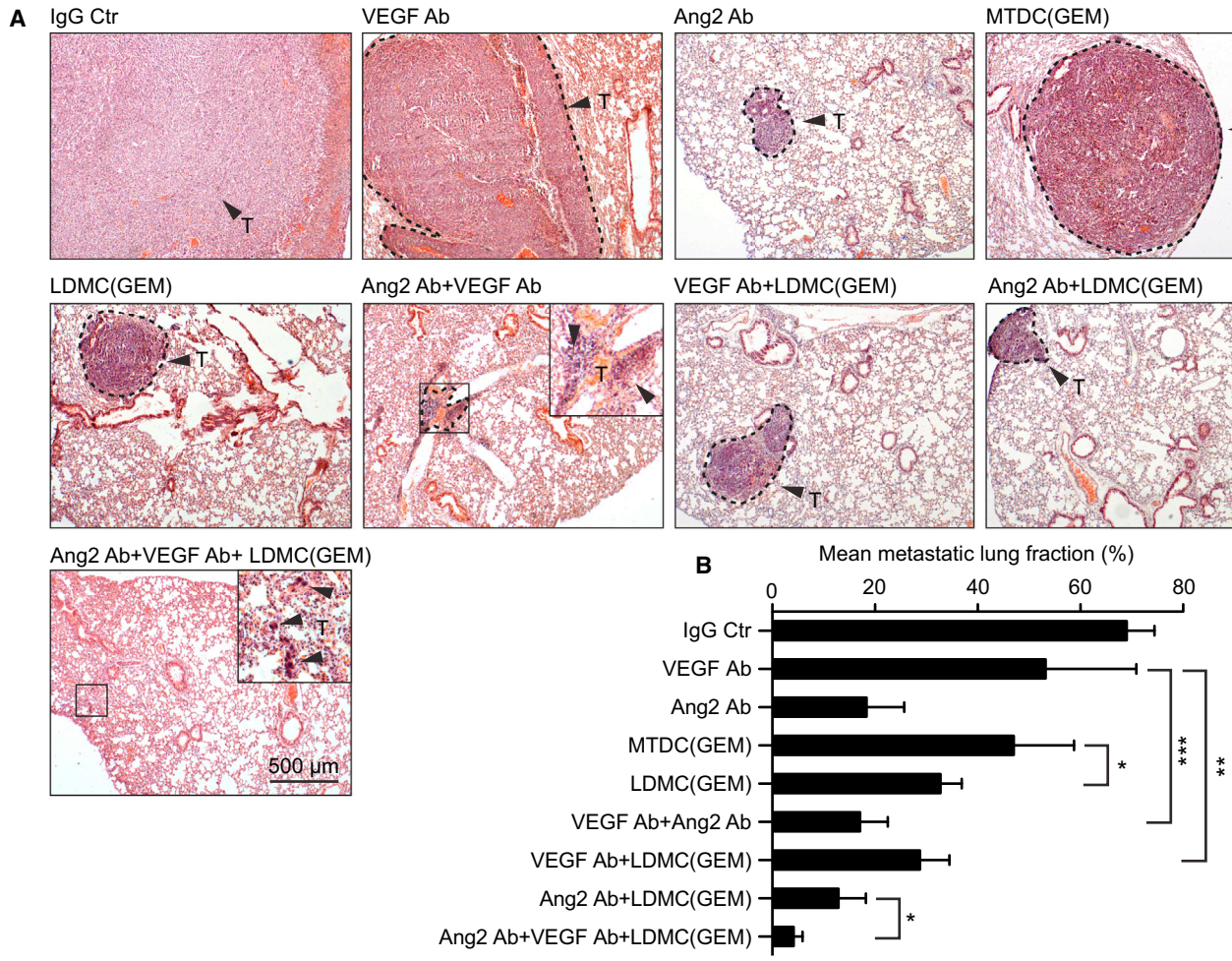

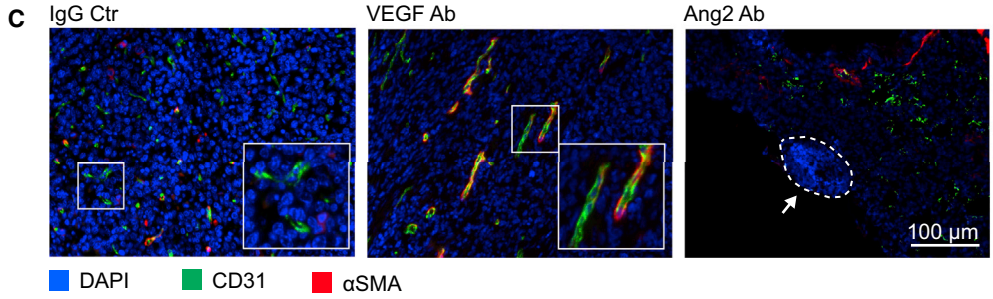

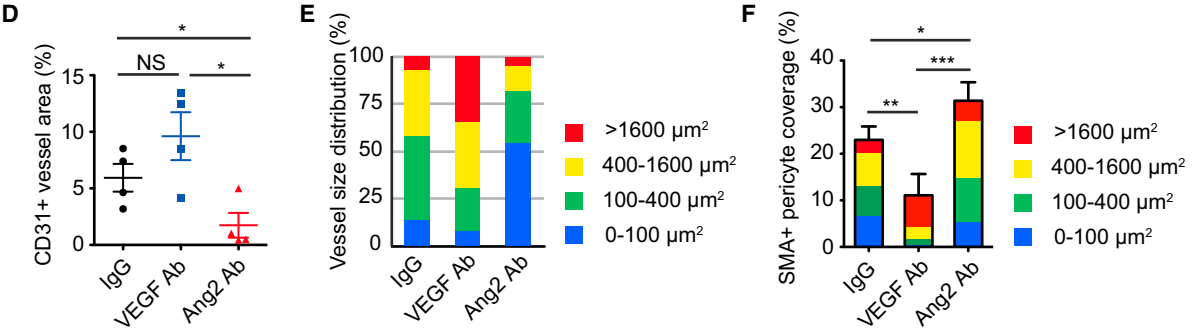

(legend on next page)

VEGF Ab refractory tumor models (Shojaei et al., 2007b, 2009). Ang2 Ab had no effect on the concentrations of Bv8 in lung metastases (Figure S6C). This led us to hypothesize that Ang2 might be critical for inducing angiogenesis in response to proangiogenic cytokines from the myeloid cells. To test this hypothesis, we performed in vitro tube formation and sprouting assays and in vivo Matrigel plug assays to evaluate the angiogenic response of Bv8 in the presence or absence of Ang2. Treatment of human cardiac microvascular ECs with Ang2 Ab decreased sprouting and vascular networks formation in the presence of exogenous Bv8 (Figures 7D, 7E, and S6D). Similarly, systemic Ab-mediated Ang2 neutralization in the Matrigel plug assay in vivo significantly reduced the vascularity in grafted Matrigel plugs containing Bv8 (Figures 7F–7H).

DISCUSSION

Antiangiogenic therapy targeting the VEGF pathway has in the past decade become part of standard tumor therapy (Carmeliet and Jain, 2011; Ferrara and Kerbel, 2005). Recently, the benefit of such therapies has also been exploited in the adjuvant setting, revealing little to no efficacy of anti-VEGF (Allegra et al., 2011; Cameron et al., 2013; de Gramont et al., 2012). Ang2-targeting therapies are presently studied as second-generation antiangiogenic drugs that combine well with anti-VEGF to improve the hitherto limited clinical efficacy of established antiangiogenic therapy (Holopainen et al., 2012; Kienast et al., 2013; Koh et al., 2010). The strong transcriptional regulation of Ang2 in activated ECs and its autocrine gatekeeper role on EC responsiveness led us to hypothesize that Ang2 may conceptually be an appealing candidate for postsurgical adjuvant tumor therapy.

By applying two spontaneous metastasis models, including one anti-VEGF-resistant model, we identified Ang2 in the present experimental preclinical study as an effective target for postsurgical adjuvant tumor therapy. Ang2 blockade following primary tumor resection significantly reduced the metastatic burden and exerted an antiangiogenic response with stabilized residual vasculature in metastases. Combining Ang2 Ab with chemotherapeutics interfering with recruitment of the anti-VEGF resistance-conferring myeloid cells further improved the therapeutic benefit. Mechanistically, we demonstrate that Ang2-stimulated ECs acquire an activated proinflammatory phenotype characterized by induction of autocrine STAT3 activation, subsequent upregulation of adhesion molecules such as ICAM-1, and secretion of the chemoattractant CCL2. The increase in Ang2-driven ICAM-1 may indirectly also contribute to the observed increase in CCL2 in metastases by supporting the adhesion of leukocyte subsets (notably macrophages), which may, beyond ECs, be a source of CCL2. $CCR2^{+}Tie2^{-}$ MAMs were recruited to the metastases via the induced CCL2 chemokine gradient, and the responsiveness of the endothelium to the myeloid cell-derived angiogenic cytokine Bv8 was increased in the presence of Ang2. These findings support the concept of Ang2 as a regulator of the inflammatory response and highlight the importance of the microenvironmental inflammatory milieu as a critical determinant of metastatic growth.

Whereas Ang2 is critical for the upregulation of Tie2 in Tie2-positive macrophages or their recruitment to primary tumors (De Palma and Naldini, 2011; Huang et al., 2011; Mazzieri et al., 2011), we detected Tie2-negative CCR2-positive MAMs in metastases arguing for this distinct macrophage subset to be involved in promoting metastatic growth. Recent evidence from human studies showed that Tie2-expressing macrophages do not correlate with metastasis (Goede et al., 2012; Schauer et al., 2012). In contrast, several studies have established a correlation between $CCR2^{+}$ $Tie2^{-}$ MAMs and breast cancer metastasis (Joyce and Pollard, 2009; Lu and Kang, 2009; Qian et al., 2011). Correspondingly, ECs have been identified as a source of the chemokine CCL2 (Sanchez et al., 2007), which recruits CCR2-positive macrophages. The present study established Ang2 as an endothelial regulator of CCL2 expression, as evidenced by in vitro, in vivo, and patient data set analyses.

Upon recruitment to metastases, macrophages require a suitable microenvironment for survival and adhesion. Adhesion molecules such as ICAM-1 expressed by ECs contribute to the proinflammatory milieu (Kobayashi et al., 2007). NF-κb and STAT3 signaling have previously been implicated in ICAM-1 regulation (Wung et al., 2005). However, the upstream regulation of ICAM-1 in metastases is still elusive. Our studies provide evidence for Ang2 as a regulator of NF-κb- and STAT3-mediated ICAM-1 expression in ECs and, thus, of monocytic cell adhesion. The correlation of Ang2 and ICAM-1 levels in advanced grade 2 and 3 breast cancer patient samples was consistent with these findings. Thus, the findings argue for a role of Ang2 in upregulating CCL2 and ICAM-1, which act in concert to promote CCR2+ macrophage recruitment and adhesion driving metastatic growth.

Endothelial STAT3 activation is critical for myeloid-derived angiogenesis (Kujawski et al., 2008). Interestingly, recent evidence points to the recruitment of $Cd11b^{+}Gr1^{+}$ myeloid cells as mediators of anti-VEGF therapy resistance (Shojaei et al., 2007a). These cells secrete the alternate proangiogenic cytokine

Figure 4. Comparative Analysis of Different Postsurgical Adjuvant Therapeutic Regimens in the Anti-VEGF Ab-Refractory LLC Model

Therapeutic regimens: IgG ctrl group; VEGF Ab = anti-VEGF Ab treatment; Ang2 Ab treatments; MTDC (GEM) = MTD gemcitabine chemotherapy; LDMC (GEM) = metronomic gemcitabine chemotherapy; VEGF Ab + LDMC (GEM) = combination of the two treatments; Ang2 Ab + LDMC (Gem) = combination of the two treatments, Ang2 Ab + VEGF Ab + LDMC (GEM) = combination the three treatments.

(A) Representative low-magnification histological images of lung sections (H&E staining) showing metastatic foci marked by dotted line and/or T with black arrowhead. The inset shows micrometastatic foci that failed to grow in the combination therapeutic regimen.

(B) Quantification of mean metastatic lung fraction analyzed by digitized image analysis using Fiji software (n = 9 mice).

(C) Representative immunohistochemical images of CD31- and αSMA-stained lung sections from different treatment groups to visualize blood vessels (CD31) and mural cells (αSMA). Insets show magnified images of the vasculature.

(D–F) Quantification and characterization of vasculature in different antiangiogenic therapy treatment groups (n = 4 mice). (D) Vessel area as percentage of total area. (E) Analysis of vessel size distribution within the vascularized area. (F) Percentage of covered vessels and size distribution of covered vessels.

Values are mean ± SD; $^{*}p \leq 0.05$, $^{**}p \leq 0.01$, $^{***}p \leq 0.001$, ns = nonsignificant. Each experiment was performed twice. The data from one representative experiment are presented in the figure. See also Figure S3.

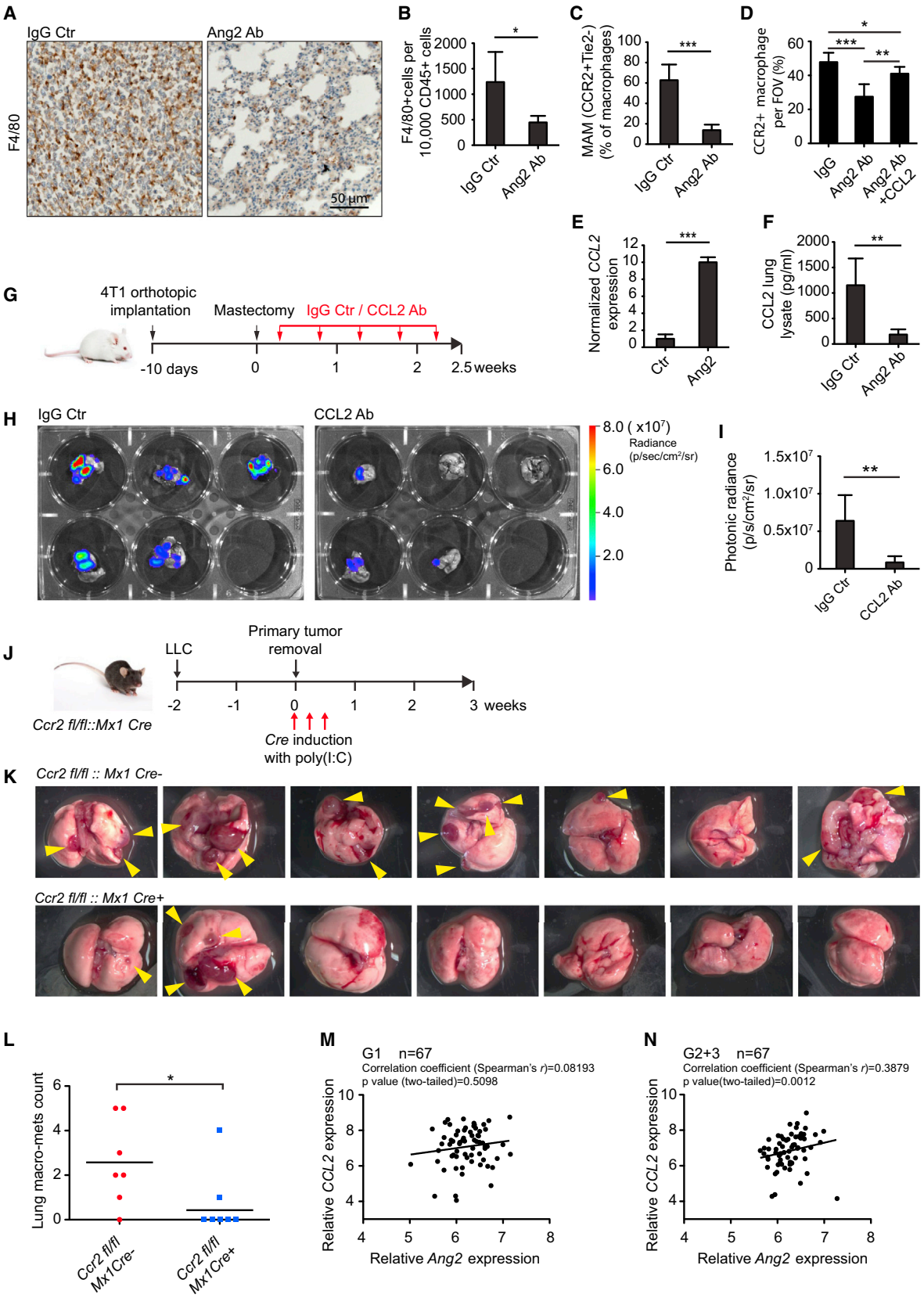

(legend on next page)

Bv8/PK2, which induces a refractory vasculature characterized by large vessels in a STAT3-dependent manner (Helfrich et al., 2010; Qu et al., 2012). The involvement of endothelial STAT3 activation in myeloid-driven angiogenesis and the reduced vascularization of growing metastases upon Ang2 Ab treatment in the anti-VEGF-refractory model led us to hypothesize that Ang2-mediated STAT-3 activation might be contributing to treatment-refractory angiogenesis. Ang2 neutralization inhibited Bv8-mediated angiogenesis, suggesting that refractory angiogenesis is caused not only by recruited myeloid cell-derived Bv8/PK2 but also by EC responsiveness to myeloid cell-derived angiogenic cytokines. These findings provide experimental evidence for a potential role of Ang2 in anti-VEGF-refractory angiogenesis in the metastatic setting, as has recently been shown in a primary tumor model (Rigamonti et al., 2014). Notably, higher Ang2 serum levels have been associated with poor prognosis in patients undergoing anti-VEGF therapy (Goede et al., 2010; Kim et al., 2013).

Considering the promising clinical studies with reduced adverse effects, LDMC may be an attractive therapeutic modality for adjuvant therapy in comparison with MTDC (Dellapasqua et al., 2008; Garcia et al., 2008). Ang2 Ab and LDMC (PTX) had better efficacy in the orthotopic breast cancer model in the adjuvant setting compared with MTDC (PTX). Moreover, the combination of Ang2 Ab and LDMC (PTX) had improved efficacy compared with Ang2 Ab alone. LDMC (PTX) was found to significantly affect the mobilization of tumor-promoting myeloid cells. A subset of these cells ($Cd11b^{+}Gr1^{+}$) has been associated with refractory angiogenesis as described earlier. We could show that angiogenesis induced by cytokines from these cells is blunted in an Ang2-deficient microenvironment, but recruitment of these cells was not affected by Ang2 neutralization. Furthermore, gemcitabine reduced recruitment of these resistance-mediating myeloid cells. The triple combination of LDMC (GEM), Ang2 Ab, and VEGF Ab further improved the therapeutic efficacy compared with Ang2 Ab and VEGF Ab, as evidenced by significantly lowered metastatic load. The reduction in myeloid cells after gemcitabine coincided with a decrease in plasma GCSF, consistent with a link between the two.

In conclusion, this study (1) has shed important therapy-relevant insights into the mechanisms of tumor progression and metastasis and (2) reports preclinical proof-of-principle experiments establishing a rationale for the combination of Ang2 Ab therapy with LDMC. Ang2 not only controls the recruitment of tumor-promoting MAMs but also affects the angiogenic response to myeloid-derived proangiogenic cytokines, such as Bv8, which contributes to anti-VEGF refractoriness. Ang2 thereby contributes to tumor progression by linking the metastatic inflammasome and the angiogenic program. Mechanistically, Ang2 is a multifaceted endotheliotropic cytokine. Genetic experiments have provided compelling evidence for a primary function of autocrine-acting Ang2 as an inhibitor of Ang1/Tie2 signaling (Augustin et al., 2009), and the findings of this study are well compatible with this model. Yet Ang2 has also been reported to act as a partial agonist of Tie2; that is, it can activate Tie2 as a weak agonist in the absence of the strong agonist Ang1 (Daly et al., 2013; Yuan et al., 2009). Moreover, angiogenically activated ECs downregulate the Ang receptor Tie2, and Ang2 has been shown to activate Tie2low ECs in an integrin-dependent manner (Felcht et al., 2012). Thus, Ang2 signaling appears to be much more complex than has previously been anticipated, and it may in a context-dependent manner be able to exert rather diverse and even opposing functions. As such, although a detailed mechanistic analysis of the intracellular downstream mechanisms of Ang2 signaling was not the focus of this study, the findings provide a compelling preclinical rationale for the mechanism-based combination of Ang2 Ab therapy and LDMC as a potential adjuvant maintenance therapy following surgical

Figure 5. Effect of Ang2 Ab on Endothelial CCL2 Expression and Recruitment of $CCR2^{+}$ MAMs

(A) Representative images of $F4/80^{+}$ cells in metastatic foci of lung in 4T1 orthotopic breast cancer model detected by DAB staining.

(B and C) Flow cytometric analysis of lung metastases-derived cell fractions from control IgG- or Ang2 Ab-treated mice (orthotopic 4T1 model). (B) Quantification of $F4/80^{+}$ macrophages infiltrating the lung metastases (n = 5 mice). (C) Quantification of $CCR2^{+}$ $Tie2^{-}$ macrophages relative to total macrophages in the lung metastases (n = 5 mice).

(D) Quantification of infiltrating $CCR2^{+}$ macrophages (MAMs) to Matrigel plugs containing serum from IgG- or Ang2 Ab-treated mice. Mice were treated after mastectomy (orthotopic 4T1 model) for 10 days before serum collection, and the Matrigel plug assay was performed for 1 week. Additionally, recombinant CCL2 was added to another group with Ang2 Ab-treated serum to evaluate if CCL2 can rescue the Ang2 blockade effect (n = 6 mice).

(E) Effect of recombinant Ang2 stimulation on *CCL2* expression (quantitative PCR analysis of cultured HUVECs). Ang2 led to a strong upregulation of *CCL2* expression (n = 3 replicates).

(F) Effect of Ang2 Ab treatment on the local concentrations of CCL2 (ELISA of lysate from lung metastases) in postsurgically treated tumor bearing mice (n = 5 mice).

(G) Schematic representation of experimental protocol. 4T1-luc tumors grown orthotopically in the third right mammary fat pad were surgically removed after 10 days (average tumor size 250 mm^3), after which therapy was initiated with the mouse CCL2 Ab or control IgG treatment. Mice were sacrificed after 2.5 weeks of treatment.

(H) Bioluminescence images from ex vivo imaging of mouse lungs immediately after sacrifice.

(I) Quantification of ex vivo bioluminescence imaging reflecting the metastatic load in lungs after IgG or CCL2 Ab treatment (n = 5 mice).

(J) Schematic representation of experimental protocol. Primary tumors (subcutaneous LLC) were grown for 2 weeks in $Ccr2^{flox/flox}$::*Mx1 Cre*-negative and $Ccr2^{flox/flox}$::*Mx1 Cre*-positive mice, after which they were surgically removed (average tumor size 360 mm^3). Following surgery, mice were (irrespective of genotype) treated with three doses of Poly I:C for Cre induction. Mice were sacrificed after another 3 weeks.

(K) Images of mouse lungs from both groups post sacrifice. The yellow arrowheads mark macroscopic metastases.

(L) Scatterplot showing quantification and distribution of macroscopic lung metastases in $Ccr2^{flox/flox}$::*Mx1 Cre*-negative and $Ccr2^{flox/flox}$::*Mx1 Cre*-positive mice after 3 weeks of Cre induction in adjuvant settings (n = 7 mice).

(M) Correlation analysis between *Ang2* and *CCL2* expression profiles in nonmetastatic breast cancer patient samples (grade 1) using the GSE3494 data set (n = 67).

(N) Correlation analysis between *Ang2* and *CCL2* expression profiles in advanced breast cancer samples (grades 2 and 3) using the GSE3494 data set (n = 67).

Values are mean ± SD unless otherwise indicated; *$p \leq 0.05$, **$p \leq 0.01$, ***$p \leq 0.001$, ns = nonsignificant. See also Figure S4.

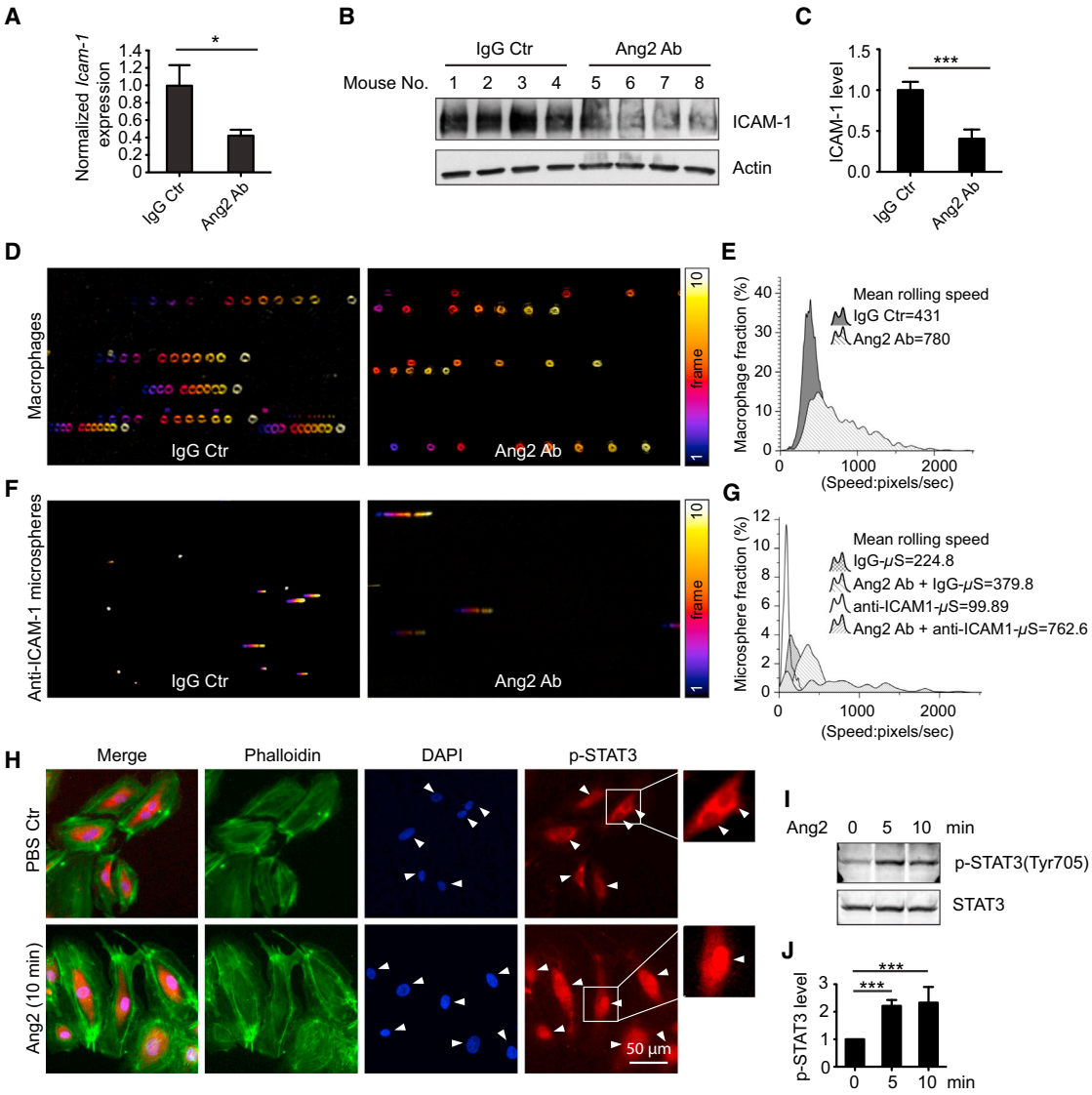

Figure 6. Ang2-Mediated Upregulation of ICAM-1 Promotes Recruitment of Macrophages

(A) Quantitative RT-PCR analysis of whole-lung lysates 24 hr after tail vein injection of 1 × 10^6 LLC tumor cells and following IgG or Ang2 Ab treatment.

(B) Western blot analysis of lysates from lung metastases originating from LLC model and adjuvant treatment with IgG or Ang2 Ab.

(C) Quantification of ICAM-1 protein expression.

(D) Velocity distribution of macrophages flowing over a HUVEC-coated parallel flow chamber. The HUVEC-coated chambers were treated with IgG (left) or Ang2 Ab (right) for 12 hr and then subjected to continuous flow of macrophages at a rate of 30 μl/min over a period of 1 min. The captured videos were processed with Fiji software. Flow velocities were recorded as pixel per second (1.4 μm/pixel). The images show representative sequences of a 0.34 s segment of rolling macrophages over a HUVEC-coated parallel flow chamber, representing a 10-frame sequence recorded at 29.97 frames/s. The sequences were processed using Fiji's edge detection and temporal color-code algorithms. Consequently, cells of the same color are part of the same frame. The distance between the differently colored macrophages was directly proportional to their rolling velocities. See also Movies S1 and S2.

(E) Quantification of macrophage velocity distribution shown in (D).

(F) Velocity distribution of microspheres (microseconds) flowing over a HUVEC-coated parallel flow chamber. The HUVEC-coated chambers were treated with either IgG or Ang2 Ab for 12 hr and then subjected to continuous flow of microspheres conjugated to either IgG or anti-ICAM-1 antibodies at a rate of 30 μl/min over a period of 1 min. The images show representative sequences of ICAM-1 Ab-conjugated microspheres rolling over IgG (left) or Ang2 Ab (right) treated HUVECs. The captured videos were processed with Fiji and analyzed as outlined in (D). See also Movies S3and S4.

(G) Quantification of macrophage velocity distribution shown in (F).

(H) Representative images showing nuclear translocation of p-STAT3 (red) into nuclei stained by DAPI (blue) and cytoskeletal Phallaoidin (green) in HUVECs upon stimulation by rhAng2 or control PBS (n = 3 replicates).

(I) Representative western blot analysis of STAT-3 phosphorylation (Tyr 705) after stimulation of HUVECs with rhAng2 (n = 5 replicates).

(J) Quantification of the ratio of p-STAT-3 to total STAT-3 protein expression normalized to control (n = 5 replicates) (see also Figure S5).

Values are mean ± SD. *p ≤ 0.05; **p ≤ 0.01; ***p ≤ 0.001.

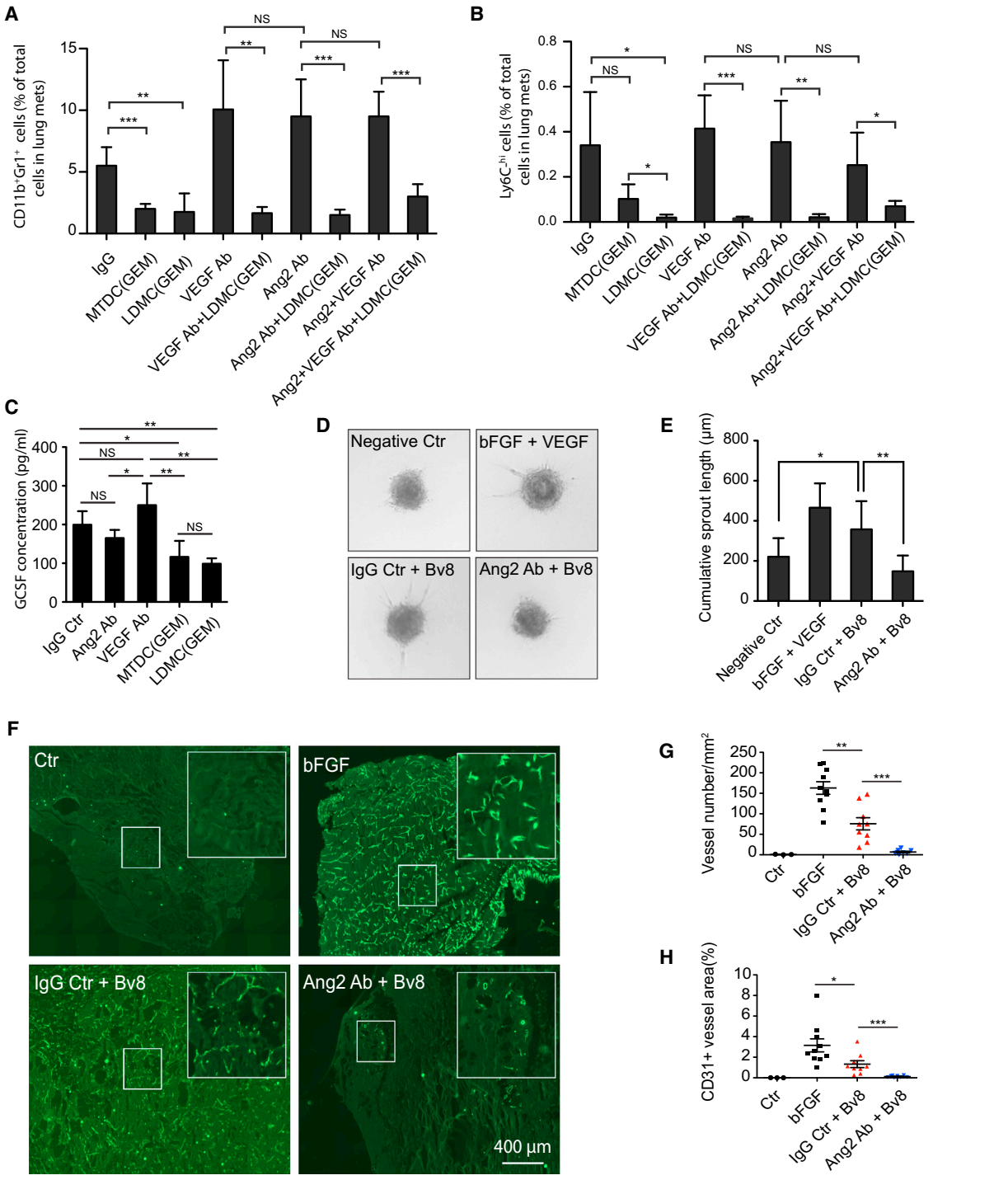

Figure 7. Evaluation of Myeloid-Derived CD11b$^+$Gr1$^+$Ly6C^{hi} Cells and Effect of Ang2 Ab on Bv8-Mediated Angiogenesis

(A and B) Effect of various therapeutic regimens on recruitment of mobilized CD11b$^+$Gr1$^+$ (A) and Cd11b$^+$Gr1$^+$Ly6C^{hi} (B) cells to the metastases. Quantification reflects the resistance conferring cells as percentage of total cells of lung metastases-derived cell suspensions from anti-VEGF-refractory LLC model. Therapeutic regimens: IgG = control IgG group; VEGF Ab = anti-VEGF Ab treatment; Ang2 Ab = anti-Ang2 Ab treatment; MTD (GEM) = MTD gemcitabine chemotherapy; LDMC (GEM) = metronomic gemcitabine chemotherapy; VEGF Ab + LDMC (GEM) = combination of the two treatments; Ang2 Ab + LDMC (Gem) = combination of the two treatments; Ang2 Ab + VEGF Ab + LDMC (GEM) = combination of the three treatments (n = 5 mice).

(C) Effect of different monotherapies on serum protein levels of GCSF, the major mobilization factor, as analyzed by ELISA (n = 5 mice).

(D and E) Evaluation of human cardiac microvascular EC sprouting induced by Bv8, the major proangiogenic cytokine produced by CD11b$^+$Gr1$^+$ cells in the presence of control IgG or Ang2 Ab. bFGF+VEGF served as positive control. The experiment was repeated three times, and 10 spheroids were evaluated each time per condition. (D) Representative images from the sprouting assay. (E) Corresponding quantification of cumulative sprout length (micrometers). In vivo

(legend continued on next page)

removal of the primary tumor or debulking pharmacotherapy, even in anti-VEGF-refractory tumors.

EXPERIMENTAL PROCEDURES

Animal Studies

C57Bl6 or severe combined immunodeficient (SCID) mice were used for the animal studies. All animal experiments were performed according to the ethical guidelines of the local animal welfare committee (Regierungspräsidum Karlsruhe).

Tumor Models

For the LLC model, LLC cells (1×10^6) were implanted subcutaneously in the flank region of 6- to 8-week-old C57Bl6 mice. Primary tumors were surgically removed after 2 weeks of growth (average tumor size 360 mm^3), and mice were randomized in the different treatment groups. Mice were treated with either Ang2 Ab or control IgG for 3 weeks, after which the mice were sacrificed and the lungs were harvested and processed for histological analysis. A third cohort of mice was sacrificed immediately after surgery to assess any baseline metastatic burden at the time of surgery. For the orthotopic breast cancer model, 4t1-luc cells (1×10^6) were implanted in the third right mammary fat pad of SCID mice (Charles River Laboratories). Mastectomy was performed 10 days after tumor cell inoculation, and the mice were randomized in the different treatment groups (see below). During the course of therapy, regular in vivo monitoring of metastatic growth was accomplished using the IVIS-200 imaging system. The animals were sacrificed at completion of the experiments, and lungs, femurs, and blood were collected for further analysis.

Adverse Effect Analysis and Survival Studies

The 4T1 orthotopic breast cancer model was used for adverse effect and survival studies. Adverse effect evaluation experiments were continued for a period of 2 weeks after mastectomy. Survival studies were performed until natural death of the mice or until the mice needed to be sacrificed for ethical reasons. Survival index plots were generated using GraphPad Prism. Body weight was monitored regularly during the course of the toxicity studies. Upon completion of the each experiment, ovaries and femurs were collected for further evaluation of reproductive toxicity and myelosuppression, respectively.

Additional Animal Experiments

Details of additional animal experiments (Matrigel plug assay, tail vein metastasis model) and treatment regimens are outlined in Supplemental Experimental Procedures.

Ex Vivo Analytical Assays and Cellular Experiments

Details of the histological analyses, immunohistochemical procedures, flow cytometric analyses used to study metastases, and cellular experiments and biochemical analyses are outlined in Supplemental Experimental Procedures.

Statistical Analysis of Data

All data are presented as mean ± SD (unless otherwise stated). Comparisons between different groups were made using Student's t test, ANOVA, and the Mann-Whitney test, as appropriate. Correlation analysis was performed in Prism using the published data set accessible through Gene Expression Omnibus series accession number GSE3494 (Miller et al., 2005). To compare groups of equal numbers of patients, a random number was assigned to each sample using the RANDOM function in Microsoft Excel, and the first 67 samples per group were included in the correlation analysis.

SUPPLEMENTAL INFORMATION

Supplemental Information includes Supplemental Experimental Procedures, six figures, and four movies and can be found with this article online at http://dx.doi.org/10.1016/j.ccell.2014.11.005.

AUTHOR CONTRIBUTIONS

K.S., J.H., and H.G.A. designed the experiments, analyzed data, and wrote the manuscript; K.S., J.H., C.K., S.S., M.T., S.S.K., M.J., and E.B. performed the experiments and analyzed data. M.T. and M.P. provided essential reagents and contributed to the writing of the manuscript.

ACKNOWLEDGMENTS

We gratefully acknowledge the excellent technical support of Dorothee Terhardt and Maria Riedel (both of DKFZ Heidelberg) as well as support from the DKFZ Laboratory Animal Facility and the DKFZ Light Microscopy Core Facilities. We would also like to acknowledge Sabine Imhof-Jung and Kay-Gunnar Stubenrauch (both of Roche Diagnostics) for the generation of murinized Ang2 and VEGF antibodies. This work was supported by grants from the Helmholtz Alliance Preclinical Comprehensive Cancer Center (to M.P. and H.G.A.), the Cooperation in Cancer Research of the German Cancer Research Center and Israeli Ministry of Science and Technology (to H.G.A.), and the Cooperation in Cancer Research of the German Cancer Research Center and Karolinska Institute (to H.G.A.), the SFB-TR23 Vascular Differentiation and Remodeling (project A3 to H.G.A.), Deutsche Krebshilfe (to M.P.), and the EU FP7 program InflaCare (to M.P.). H.G.A. is supported by an endowed chair from the Aventis Foundation. M.T. is an employee of Roche Diagnostics (Penzberg, Germany).

Received: December 14, 2012
Revised: April 10, 2014
Accepted: November 12, 2014
Published: December 8, 2014

REFERENCES

Allegra, C.J., Yothers, G., O'Connell, M.J., Sharif, S., Petrelli, N.J., Colangelo, L.H., Atkins, J.N., Seay, T.E., Fehrenbacher, L., Goldberg, R.M., et al. (2011). Phase III trial assessing bevacizumab in stages II and III carcinoma of the colon: results of NSABP protocol C-08. J. Clin. Oncol. *29*, 11–16.

Augustin, H.G., Koh, G.Y., Thurston, G., and Alitalo, K. (2009). Control of vascular morphogenesis and homeostasis through the angiopoietin-Tie system. Nat. Rev. Mol. Cell Biol. *10*, 165–177.

Cameron, D., Brown, J., Dent, R., Jackisch, C., Mackey, J., Pivot, X., Steger, G.G., Suter, T.M., Toi, M., Parmar, M., et al. (2013). Adjuvant bevacizumab-containing therapy in triple-negative breast cancer (BEATRICE): primary results of a randomised, phase 3 trial. Lancet Oncol. *14*, 933–942.

Carmeliet, P., and Jain, R.K. (2011). Molecular mechanisms and clinical applications of angiogenesis. Nature *473*, 298–307.

Daly, C., Eichten, A., Castanaro, C., Pasnikowski, E., Adler, A., Lalani, A.S., Papadopoulos, N., Kyle, A.H., Minchinton, A.I., Yancopoulos, G.D., and Thurston, G. (2013). Angiopoietin-2 functions as a Tie2 agonist in tumor models, where it limits the effects of VEGF inhibition. Cancer Res. *73*, 108–118.

de Gramont, A., Van Cutsem, E., Schmoll, H.J., Tabernero, J., Clarke, S., Moore, M.J., Cunningham, D., Cartwright, T.H., Hecht, J.R., Rivera, F., et al. (2012). Bevacizumab plus oxaliplatin-based chemotherapy as adjuvant

evaluation of the ability of Ang2 Ab or control IgG to interfere with Bv8-induced angiogenesis in Matrigel plug assay. Matrigel plugs were preloaded with Bv8, bFGF (positive control), or saline (negative control). Mice with Bv8 preloaded plugs were either treated with control IgG or Ang2 Ab for 10 days.
(F) Representative images of Matrigel plug sections stained for CD31 (green) to analyze angiogenesis.
(G) Quantification of the number of vessels per unit area (square millimeters) of the Matrigel plugs (n = 10 plugs).
(H) Quantification of CD31-positive area as percentage of total Matrigel plug area (n = 10 plugs).
Values are mean ± SD; *$p \leq 0.05$, **$p \leq 0.01$, ***$p \leq 0.001$, ns = nonsignificant. Each experiment was performed at least twice unless indicated otherwise. Data from one representative experiment are presented in the figure. See also Figure S6.

treatment for colon cancer (AVANT): a phase 3 randomised controlled trial. Lancet Oncol. *13*, 1225–1233.

De Palma, M., and Naldini, L. (2011). Angiopoietin-2 TIEs up macrophages in tumor angiogenesis. Clin. Cancer Res. *17*, 5226–5232.

Dellapasqua, S., Bertolini, F., Bagnardi, V., Campagnoli, E., Scarano, E., Torrisi, R., Shaked, Y., Mancuso, P., Goldhirsch, A., Rocca, A., et al. (2008). Metronomic cyclophosphamide and capecitabine combined with bevacizumab in advanced breast cancer. J. Clin. Oncol. *26*, 4899–4905.

Demicheli, R., Retsky, M.W., Hrushesky, W.J., Baum, M., and Gukas, I.D. (2008). The effects of surgery on tumor growth: a century of investigations. Ann. Oncol. *19*, 1821–1828.

Ebos, J.M., Lee, C.R., Cruz-Munoz, W., Bjarnason, G.A., Christensen, J.G., and Kerbel, R.S. (2009). Accelerated metastasis after short-term treatment with a potent inhibitor of tumor angiogenesis. Cancer Cell *15*, 232–239.

Felcht, M., Luck, R., Schering, A., Seidel, P., Srivastava, K., Hu, J., Bartol, A., Kienast, Y., Vettel, C., Loos, E.K., et al. (2012). Angiopoietin-2 differentially regulates angiogenesis through TIE2 and integrin signaling. J. Clin. Invest. *122*, 1991–2005.

Ferrara, N., and Kerbel, R.S. (2005). Angiogenesis as a therapeutic target. Nature *438*, 967–974.

Garcia, A.A., Hirte, H., Fleming, G., Yang, D., Tsao-Wei, D.D., Roman, L., Groshen, S., Swenson, S., Markland, F., Gandara, D., et al. (2008). Phase II clinical trial of bevacizumab and low-dose metronomic oral cyclophosphamide in recurrent ovarian cancer: a trial of the California, Chicago, and Princess Margaret Hospital phase II consortia. J. Clin. Oncol. *26*, 76–82.

Gerald, D., Chintharlapalli, S., Augustin, H.G., and Benjamin, L.E. (2013). Angiopoietin-2: an attractive target for improved antiangiogenic tumor therapy. Cancer Res. *73*, 1649–1657.

Goede, V., Coutelle, O., Neuneier, J., Reinacher-Schick, A., Schnell, R., Koslowsky, T.C., Weihrauch, M.R., Cremer, B., Kashkar, H., Odenthal, M., et al. (2010). Identification of serum angiopoietin-2 as a biomarker for clinical outcome of colorectal cancer patients treated with bevacizumab-containing therapy. Br. J. Cancer *103*, 1407–1414.

Goede, V., Coutelle, O., Shimabukuro-Vornhagen, A., Holtick, U., Neuneier, J., Koslowsky, T.C., Weihrauch, M.R., von Bergwelt-Baildon, M., and Hacker, U.T. (2012). Analysis of Tie2-expressing monocytes (TEM) in patients with colorectal cancer. Cancer Invest. *30*, 225–230.

Hashizume, H., Falcón, B.L., Kuroda, T., Baluk, P., Coxon, A., Yu, D., Bready, J.V., Oliner, J.D., and McDonald, D.M. (2010). Complementary actions of inhibitors of angiopoietin-2 and VEGF on tumor angiogenesis and growth. Cancer Res. *70*, 2213–2223.

Helfrich, I., Scheffrahn, I., Bartling, S., Weis, J., von Felbert, V., Middleton, M., Kato, M., Ergün, S., Augustin, H.G., and Schadendorf, D. (2010). Resistance to antiangiogenic therapy is directed by vascular phenotype, vessel stabilization, and maturation in malignant melanoma. J. Exp. Med. *207*, 491–503.

Holash, J., Maisonpierre, P.C., Compton, D., Boland, P., Alexander, C.R., Zagzag, D., Yancopoulos, G.D., and Wiegand, S.J. (1999). Vessel cooption, regression, and growth in tumors mediated by angiopoietins and VEGF. Science *284*, 1994–1998.

Holopainen, T., Saharinen, P., D'Amico, G., Lampinen, A., Eklund, L., Sormunen, R., Anisimov, A., Zarkada, G., Lohela, M., Heloterä, H., et al. (2012). Effects of angiopoietin-2-blocking antibody on endothelial cell-cell junctions and lung metastasis. J. Natl. Cancer Inst. *104*, 461–475.

Huang, H., Lai, J.Y., Do, J., Liu, D., Li, L., Del Rosario, J., Doppalapudi, V.R., Pirie-Shepherd, S., Levin, N., Bradshaw, C., et al. (2011). Specifically targeting angiopoietin-2 inhibits angiogenesis, Tie2-expressing monocyte infiltration, and tumor growth. Clin. Cancer Res. *17*, 1001–1011.

Joyce, J.A., and Pollard, J.W. (2009). Microenvironmental regulation of metastasis. Nat. Rev. Cancer *9*, 239–252.

Kienast, Y., Klein, C., Scheuer, W., Raemsch, R., Lorenzon, E., Bernicke, D., Herting, F., Yu, S., The, H.H., Martarello, L., et al. (2013). Ang-2-VEGF-A CrossMab, a novel bispecific human IgG1 antibody blocking VEGF-A and Ang-2 functions simultaneously, mediates potent antitumor, antiangiogenic, and antimetastatic efficacy. Clin. Cancer Res. *19*, 6730–6740.

Kim, S., Dobi, E., Jary, M., Monnien, F., Curtit, E., Nguyen, T., Lakkis, Z., Heyd, B., Fratte, S., Cléau, D., et al. (2013). Bifractionated CPT-11 with LV5FU2 infusion (FOLFIRI-3) in combination with bevacizumab: clinical outcomes in first-line metastatic colorectal cancers according to plasma angiopoietin-2 levels. BMC Cancer *13*, 611.

Kobayashi, H., Boelte, K.C., and Lin, P.C. (2007). Endothelial cell adhesion molecules and cancer progression. Curr. Med. Chem. *14*, 377–386.

Koh, Y.J., Kim, H.Z., Hwang, S.I., Lee, J.E., Oh, N., Jung, K., Kim, M., Kim, K.E., Kim, H., Lim, N.K., et al. (2010). Double antiangiogenic protein, DAAP, targeting VEGF-A and angiopoietins in tumor angiogenesis, metastasis, and vascular leakage. Cancer Cell *18*, 171–184.

Kujawski, M., Kortylewski, M., Lee, H., Herrmann, A., Kay, H., and Yu, H. (2008). Stat3 mediates myeloid cell-dependent tumor angiogenesis in mice. J. Clin. Invest. *118*, 3367–3377.

Lu, X., and Kang, Y. (2009). Chemokine (C-C motif) ligand 2 engages CCR2+ stromal cells of monocytic origin to promote breast cancer metastasis to lung and bone. J. Biol. Chem. *284*, 29087–29096.

Mazzieri, R., Pucci, F., Moi, D., Zonari, E., Ranghetti, A., Berti, A., Politi, L.S., Gentner, B., Brown, J.L., Naldini, L., and De Palma, M. (2011). Targeting the ANG2/TIE2 axis inhibits tumor growth and metastasis by impairing angiogenesis and disabling rebounds of proangiogenic myeloid cells. Cancer Cell *19*, 512–526.

Miller, L.D., Smeds, J., George, J., Vega, V.B., Vergara, L., Ploner, A., Pawitan, Y., Hall, P., Klaar, S., Liu, E.T., and Bergh, J. (2005). An expression signature for p53 status in human breast cancer predicts mutation status, transcriptional effects, and patient survival. Proc. Natl. Acad. Sci. U S A *102*, 13550–13555.

Pàez-Ribes, M., Allen, E., Hudock, J., Takeda, T., Okuyama, H., Viñals, F., Inoue, M., Bergers, G., Hanahan, D., and Casanovas, O. (2009). Antiangiogenic therapy elicits malignant progression of tumors to increased local invasion and distant metastasis. Cancer Cell *15*, 220–231.

Priceman, S.J., Sung, J.L., Shaposhnik, Z., Burton, J.B., Torres-Collado, A.X., Moughon, D.L., Johnson, M., Lusis, A.J., Cohen, D.A., Iruela-Arispe, M.L., and Wu, L. (2010). Targeting distinct tumor-infiltrating myeloid cells by inhibiting CSF-1 receptor: combating tumor evasion of antiangiogenic therapy. Blood *115*, 1461–1471.

Qian, B.Z., and Pollard, J.W. (2010). Macrophage diversity enhances tumor progression and metastasis. Cell *141*, 39–51.

Qian, B.Z., Li, J., Zhang, H., Kitamura, T., Zhang, J., Campion, L.R., Kaiser, E.A., Snyder, L.A., and Pollard, J.W. (2011). CCL2 recruits inflammatory monocytes to facilitate breast-tumour metastasis. Nature *475*, 222–225.

Qu, X., Zhuang, G., Yu, L., Meng, G., and Ferrara, N. (2012). Induction of Bv8 expression by granulocyte colony-stimulating factor in CD11b+Gr1+ cells: key role of Stat3 signaling. J. Biol. Chem. *287*, 19574–19584.

Rigamonti, N., Kadioglu, E., Keklikoglou, I., Wyser Rmili, C., Leow, C.C., and De Palma, M. (2014). Role of angiopoietin-2 in adaptive tumor resistance to VEGF signaling blockade. Cell Reports *8*, 696–706.

Sanchez, O., Marcos, E., Perros, F., Fadel, E., Tu, L., Humbert, M., Dartevelle, P., Simonneau, G., Adnot, S., and Eddahibi, S. (2007). Role of endothelium-derived CC chemokine ligand 2 in idiopathic pulmonary arterial hypertension. Am. J. Respir. Crit. Care Med. *176*, 1041–1047.

Schauer, D., Starlinger, P., Reiter, C., Jahn, N., Zajc, P., Buchberger, E., Bachleitner-Hofmann, T., Bergmann, M., Stift, A., Gruenberger, T., and Brostjan, C. (2012). Intermediate monocytes but not TIE2-expressing monocytes are a sensitive diagnostic indicator for colorectal cancer. PLoS ONE *7*, e44450.

Shojaei, F., Wu, X., Malik, A.K., Zhong, C., Baldwin, M.E., Schanz, S., Fuh, G., Gerber, H.P., and Ferrara, N. (2007a). Tumor refractoriness to anti-VEGF treatment is mediated by CD11b+Gr1+ myeloid cells. Nat. Biotechnol. *25*, 911–920.

Shojaei, F., Wu, X., Zhong, C., Yu, L., Liang, X.H., Yao, J., Blanchard, D., Bais, C., Peale, F.V., van Bruggen, N., et al. (2007b). Bv8 regulates myeloid-cell-dependent tumour angiogenesis. Nature *450*, 825–831.

Shojaei, F., Wu, X., Qu, X., Kowanetz, M., Yu, L., Tan, M., Meng, Y.G., and Ferrara, N. (2009). G-CSF-initiated myeloid cell mobilization and angiogenesis

mediate tumor refractoriness to anti-VEGF therapy in mouse models. Proc. Natl. Acad. Sci. U S A *106*, 6742–6747.

Suzuki, E., Kapoor, V., Jassar, A.S., Kaiser, L.R., and Albelda, S.M. (2005). Gemcitabine selectively eliminates splenic Gr-1+/CD11b+ myeloid suppressor cells in tumor-bearing animals and enhances antitumor immune activity. Clin. Cancer Res. *11*, 6713–6721.

Turkson, J., Ryan, D., Kim, J.S., Zhang, Y., Chen, Z., Haura, E., Laudano, A., Sebti, S., Hamilton, A.D., and Jove, R. (2001). Phosphotyrosyl peptides block Stat3-mediated DNA binding activity, gene regulation, and cell transformation. J. Biol. Chem. *276*, 45443–45455.

Wung, B.S., Ni, C.W., and Wang, D.L. (2005). ICAM-1 induction by TNFalpha and IL-6 is mediated by distinct pathways via Rac in endothelial cells. J. Biomed. Sci. *12*, 91–101.

Yahata, Y., Shirakata, Y., Tokumaru, S., Yamasaki, K., Sayama, K., Hanakawa, Y., Detmar, M., and Hashimoto, K. (2003). Nuclear translocation of phosphorylated STAT3 is essential for vascular endothelial growth factor-induced human dermal microvascular endothelial cell migration and tube formation. J. Biol. Chem. *278*, 40026–40031.

Yuan, H.T., Khankin, E.V., Karumanchi, S.A., and Parikh, S.M. (2009). Angiopoietin 2 is a partial agonist/antagonist of Tie2 signaling in the endothelium. Mol. Cell. Biol. *29*, 2011–2022.

Zagzag, D., Hooper, A., Friedlander, D.R., Chan, W., Holash, J., Wiegand, S.J., Yancopoulos, G.D., and Grumet, M. (1999). In situ expression of angiopoietins in astrocytomas identifies angiopoietin-2 as an early marker of tumor angiogenesis. Exp. Neurol. *159*, 391–400.